Fire Safety Journal 163 (2026) 104843

Contents lists available at ScienceDirect

Fire Safety Journal

journal homepage: www.elsevier.com/locate/firesaf

Merging of two opposite-spreading flames on kerosene under parallel and perpendicular wind

Bo Li [a,b,c], Yangjin Shi [a], Xinyan Huang [c,*], Asif Sohail Usmani [c]

[a] Faculty of Engineering, China University of Geosciences, 388 LvMo Road, WuHan, China
[b] State Key Laboratory of Fire Science, University of Science and Technology of China, 96 JinZhai Road, Hefei, China
[c] Department of Building Environment and Energy Engineering, The Hong Kong Polytechnic University, 181 Chatham Road South, Kowloon, Hong Kong, China

ARTICLE INFO

Keywords:
Flame spread
Fire merging
Liquid fuel
Wind direction
Gas-liquid temperature

ABSTRACT

Liquid fuels such as aviation kerosene are highly flammable and volatile, showing a significant risk of fire and explosion. This work conducted experiments on the spread of two flames toward each other and merging behavior of RP-5 aviation kerosene under parallel and perpendicular winds. Under the parallel wind ($u_{\parallel}$), at $u_{\parallel} \leq$ 0.5 m/s, the dual effects of heat plume collision-induced heat dispersion and insufficient fuel vapor diffusion significantly suppressed the merging speed of two flames. At $u_{\parallel} >$ 0.5 m/s, the spread rate is enhanced by concurrent wind through flame stretching and combustion area enlargement, while the flame leading edge is continuously blown off by the opposed wind. Meanwhile, the flame merging point gradually shifts toward the leeward side with increasing $u_{\parallel}$. Under the perpendicular wind ($u_{\perp}$), spread behavior at low-wind speeds resembles that under parallel wind. At $u_{\perp} >$ 0.5 m/s, symmetric vortices are formed to improve oxygen-fuel mixing efficiency and superimpose radiant heat, which promotes the flame spread more than the concurrent wind. The gas-liquid two-phase temperature distribution reveals the dynamic heat transfer process: the gas-phase temperature rises rapidly, while the liquid-phase temperature exhibits a delayed response. Finally, a prediction model of flame spread rate is developed.

1. Introduction

The advancement of aviation technologies and naval engineering in recent decades has been accompanied by an increased incidence of liquid fuel-related fire hazards, particularly stemming from leakage scenarios [1–3]. Liquid fuels such as aviation kerosene are highly flammable and volatile, becoming readily ignitable when leaked and exposed to ignition sources. Their high fluidity further promotes the expansion of the leakage area, leading to rapid fire spread. In real fire scenarios, ambient airflow typically exacerbates the combustion process [4] by supplying ample oxidizer for flame propagation, significantly increasing uncontrollability, and potentially causing severe economic losses and casualties [5]. For example, on December 12, 2019, during maintenance of the Russian aircraft carrier Admiral Kuznetsov, a fire broke out after workers accidently ignited leaked fuel. Driven by ambient wind, the affected area rapidly expanded from 20 m^2 to 600 m^2, resulting in 2 firefighter fatalities, 14 injuries, and over 500 million RUB in losses [6]. Therefore, in-depth research on flame spread behavior under forced airflow is essential for enhancing fuel leakage fire prevention and control. During flame spread, the flame spread rate, flame morphology, and gas-liquid temperature distributions are key parameters for assessing fire hazard levels. The flame spread rate determines the speed of fire development and evacuation time windows; The evolution of flame morphology may trigger secondary ignition of adjacent leakage sources; Gas-liquid temperature variations influence fuel heat feedback and combustion intensity, thereby altering spread characteristics and heat transfer mechanisms. Regarding the impact of ambient wind on flame spread behavior, extensive research has been conducted domestically and internationally, yielding substantial findings.

Previous research primarily focused on ambient wind effects on single-source flame spread, examining the effects of wind speed and wind direction. Regarding wind speed factors, Anderson et al. [7] observed that flames tilt under wind action, thereby enhancing radiative preheating of unburned fuel, whereas convective heating is only present in the region close to the flame front. The correlations of flame tilt angle and flame height under varied concurrent wind speeds were developed

This article is part of a special issue entitled: FISJ_IAFSS 2026 published in Fire Safety Journal.

* Corresponding author.
E-mail addresses: libo93@cug.edu.cn (B. Li), xy.huang@polyu.edu.hk (X. Huang).

https://doi.org/10.1016/j.firesaf.2026.104843
Received 24 September 2025; Received in revised form 15 January 2026; Accepted 30 March 2026
Available online 12 April 2026

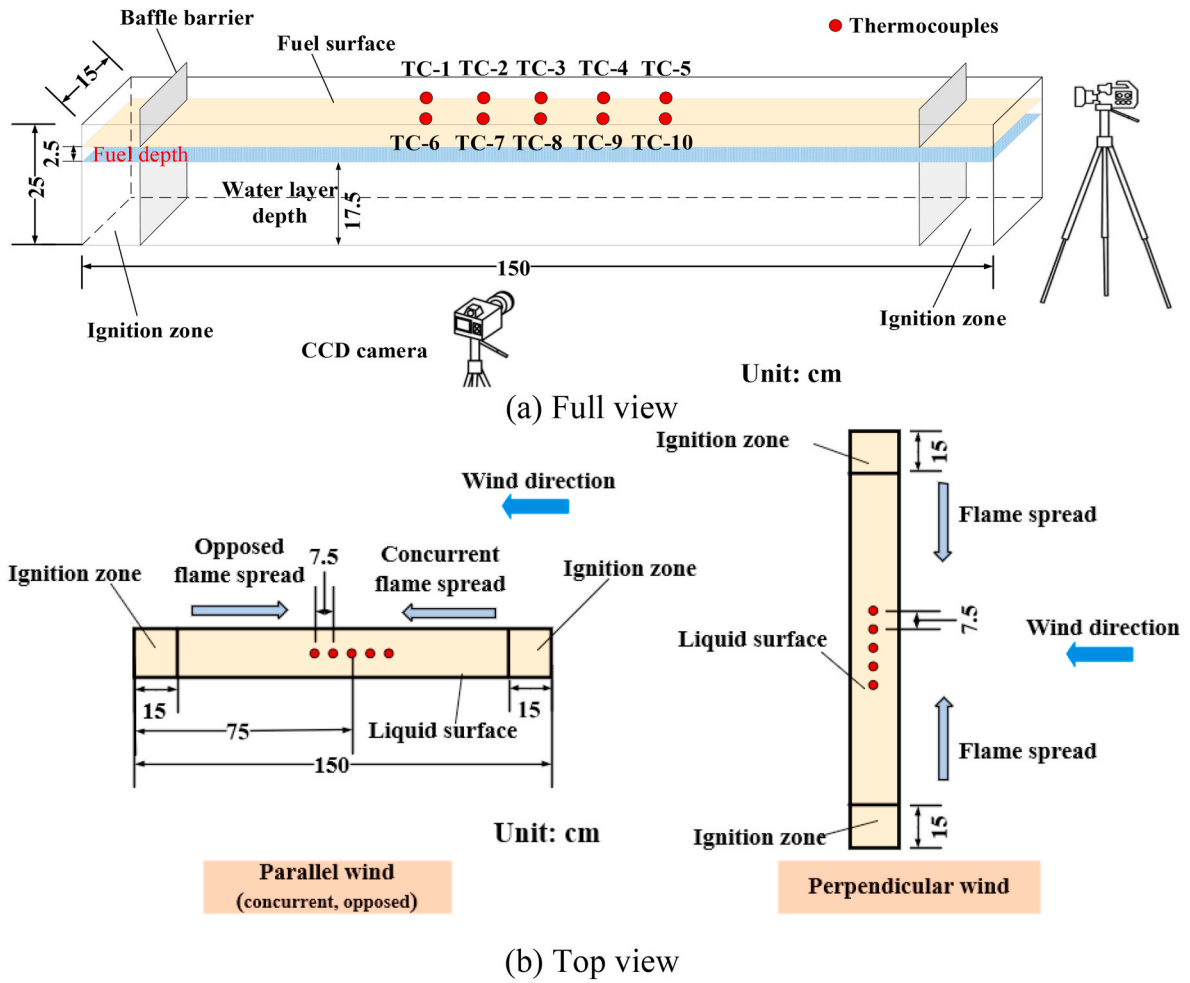

Fig. 1. Experimental setup of flame spread over liquid fuel, (a) full view, and (b) top view for applying parallel wind ($u_{\parallel}$) and perpendicular wind ($u_{\perp}$).

by Li et al. [8,9]. Burgoyne and Roberts [10] experimentally studied single-source flame spread of propanol and isoamyl alcohol in a 1 m × 12 cm channel. At low concurrent and opposed wind speeds ($u < 1$ m/s), only minor spread rate fluctuations were observed. However, when wind speed exceeded 1 m/s, the variation amplitude of the flame spread rate, V_f could reach 150%. They also indicated that when the opposed wind speed surpassed 2 m/s, V_f decreased with increasing wind speed, ultimately leading to complete suppression of combustion. Suzuki and Hirano [11] further investigated the effects of initial fuel temperature ($T_0 = 5$–30 °C) and wind speed ($u = 0$–6 m/s) on the single-source flame spread rate of methanol, reaching similar conclusions. They noted that under concurrent wind conditions, when u exceeded the spread rate under no-wind conditions, V_f approached the wind speed itself and ceased to be affected by T_0. Zamashchikov et al. [12] studied the single-source flame spread over the n-butanol surface under opposed wind conditions, likewise concluding that V_f gradually decreased with increasing u until the flame could no longer propagate, defining u at this point as the critical threshold for opposed wind flame spread. Ali et al. [13] analyzed single-source flame spread characteristics over the methanol surface under concurrent wind conditions (u= 1.3–5.1 m/s) using numerical simulation. A positive correlation between flame spread rate and u was demonstrated. This correlation was primarily attributed to enhanced oxidizer transport by concurrent wind, which promoted flame combustion and increased spread rates. This mechanism was supported by Zhu et al. [14], whose experiments on horizontal PMMA plates under concurrent winds (0-1.5 m/s) showed significantly enhanced flame-to-fuel surface heat flux, resulting in a linear relationship between V_f and wind speed. Gollner et al. [15] further summarized that increasing concurrent wind drives flames closer to the unburned fuel surface ahead of the fire front, intensifying heating effects and thereby accelerating spread rates. Recently, Mao et al. [16] investigated the gas-liquid temperature distributions during single-source kerosene flame spread under concurrent wind, setting six wind speed conditions from 0 to 6 m/s. When the wind speed exceeded a critical value (>1 m/s), the evolution patterns of gas-liquid temperatures during flame spread changed significantly: gas-phase temperature rise preceded liquid-phase heating, and liquid surface flow near the flame front essentially vanished.

Regarding the influence of wind direction on flame spread behavior, Ross et al. [17] investigated V_f of the single ignition source over a 1-butanol surface under concurrent and opposed wind (0.05 to 0.3 m/s). The distribution of the liquid temperature field was significantly influenced by wind direction. Flame pulsation frequency was primarily altered by small opposed winds, whereas minor concurrent winds effectively suppressed pulsation. Zanganeh and Moghtaderi [18] studied single-source flame spread over propanol-wetted porous sand beds (depth 13.3–39.9 mm) under concurrent and opposed wind (0–1.5 m/s). They found that the flame spread rate over the oil-soaked sand surface significantly decreased with increasing wind speed under both conditions, with the suppression effect being more pronounced under opposed wind than under concurrent wind. Li et al. [19] experimentally studied the single-source spread behavior of diesel flames under concurrent and opposed wind (0–2.065 m/s) and observed divergent behaviors: under concurrent wind, the flame spread rate (V_f) initially decreased then increased, with a critical transition at 1.725 m/s; under opposed wind, V_f was continuously suppressed. They attributed the opposed wind effect

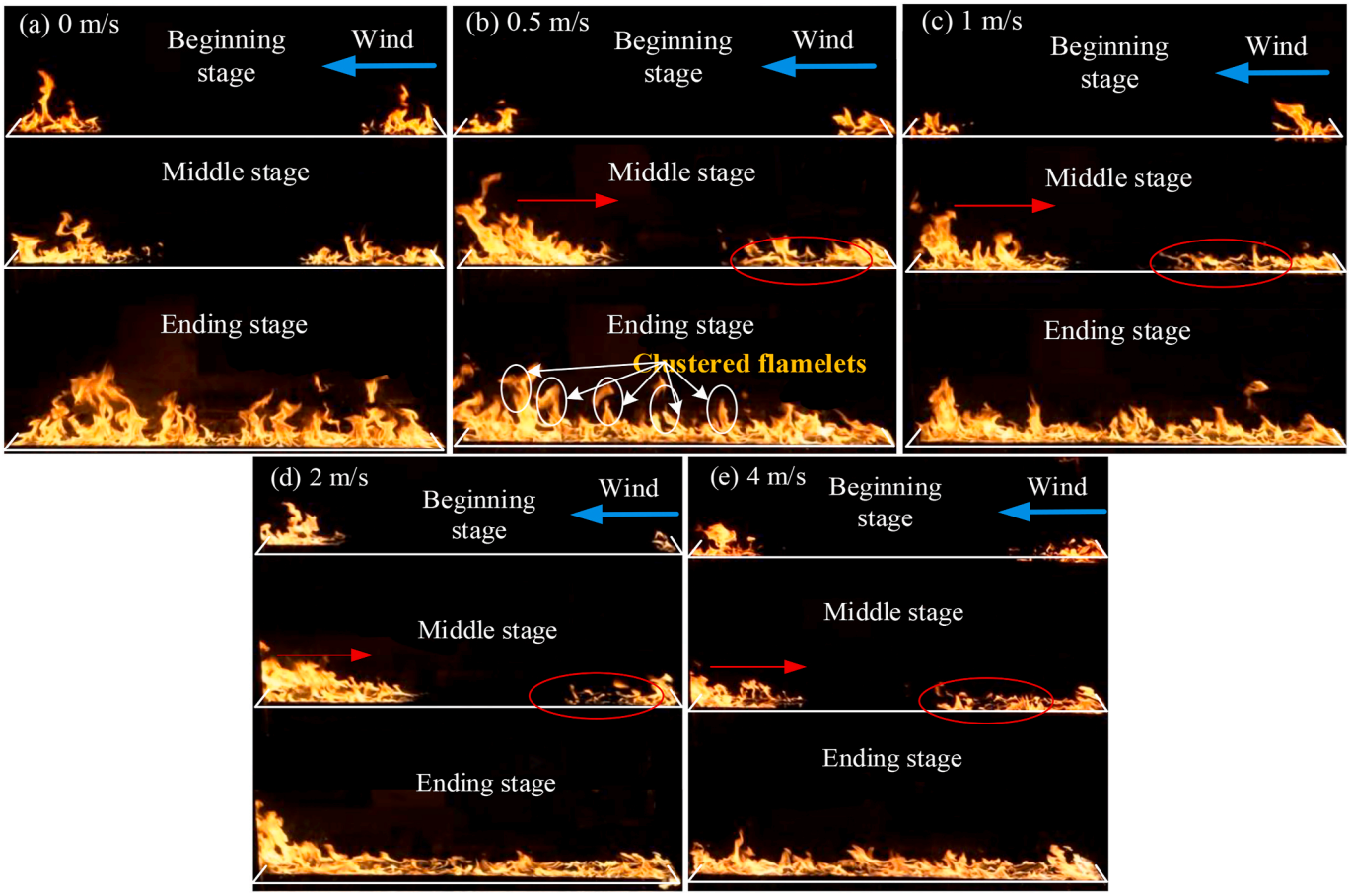

Fig. 2. The instantaneous flame spread images under parallel wind (front -view).

to weakened thermal expansion of the flame front and reduced propulsion from combustion products, which largely inhibited propagation. Huang and Gao [20] complemented this mechanism by proposing that as opposed wind speed increases, flame spread shifts to a "chemical regime," where excessive air cools the combustion front, destabilizes opposed spread, and only sustains concurrent spread. Mao et al. [21] expanded the analysis to include perpendicular wind, comparing concurrent, opposed, and perpendicular conditions. At wind speeds >1 m/s, significant directional disparities emerged in flame spread rates: concurrent wind > perpendicular wind > opposed wind, highlighting the dominant role of wind direction in dictating propagation efficiency.

Research on single-source flame spread under ambient wind is now relatively mature. In real fire scenarios, however, intense radiation frequently leads to multiple ignition sources spreading simultaneously. Liu et al. [22] proposed that multiple fires burning and merging often act as crucial steps for accelerating surface fire spread, generating large-size flames, and triggering unique spread modes. To address the influence of ambient wind on flame merging, Wadhwani et al. [23] conducted simulations to study two parallel merging wildfires under wind conditions and found that the average rate of fire spread exhibits a non-monotonic trend of first decreasing and then increasing with wind speed. Specifically, when multiple fire fronts approach each other under wind influence, restricted air entrainment and enhanced heat feedback may trigger a junction fire, whose small-angle intersection causes a sharp increase in spread rate at the intersection point [24,25].

Overall, most literature studies have focused solely on single-source flame spread, while overlooking the common flame merging phenomena. Moreover, past research emphasis predominantly centers on flame spread under parallel wind (concurrent or opposed wind), while taking insufficient attention to their dynamics under perpendicular wind. This work examined spread of two flames toward each other and merging behavior over liquid fuel (RP-5 aviation kerosene) under five wind speeds (0–4 m/s) and three wind directions (concurrent, opposed, and perpendicular). Specifically, the flame-morphology evolution and gas-liquid temperature distribution are systematically analyzed to reveal the flame spread mechanism over liquid fuel. A flame spread rate prediction model was developed based on airflow parameters and temperature features and verified against literature data. This research enriches flame spread theory and provides scientific guideline to support fire risk assessment of liquid-fuel.

2. Experimental methods

As shown in Fig. 1, a rectangular fuel pool measuring 150 cm (length) × 15 cm (width) × 25 cm (height) was employed as the flame spread apparatus, and the pool wall material was 304 stainless steel (thickness: 2 mm) with high thermal stability. RP-5 aviation kerosene was served as the fuel layer. The 2.5 cm fuel depth was determined based on preliminary experiments (3 depths: 1 cm, 2.5 cm, 4 cm). It balances stable combustion and optimal fuel depletion during tests, ensuring consistent spread behavior. To mimic both marine and land spill scenarios, a 17.5 cm deep water buffer layer was created at the base of fuel pool. The water base can maintain isothermal conditions to eliminate temperature-induced fuel convection, and minimize pool interference (e.g., uneven heat conduction through pool walls, unintended liquid motion) —an essential optimization to ensure the reliability and interpretability of the study's core findings, namely the effects of wind speed and direction on the spreading and merging behavior of two opposing flames. As an extension of the present work, the detailed heat transfer mechanisms within the fuel layer or from the pool to the underlying

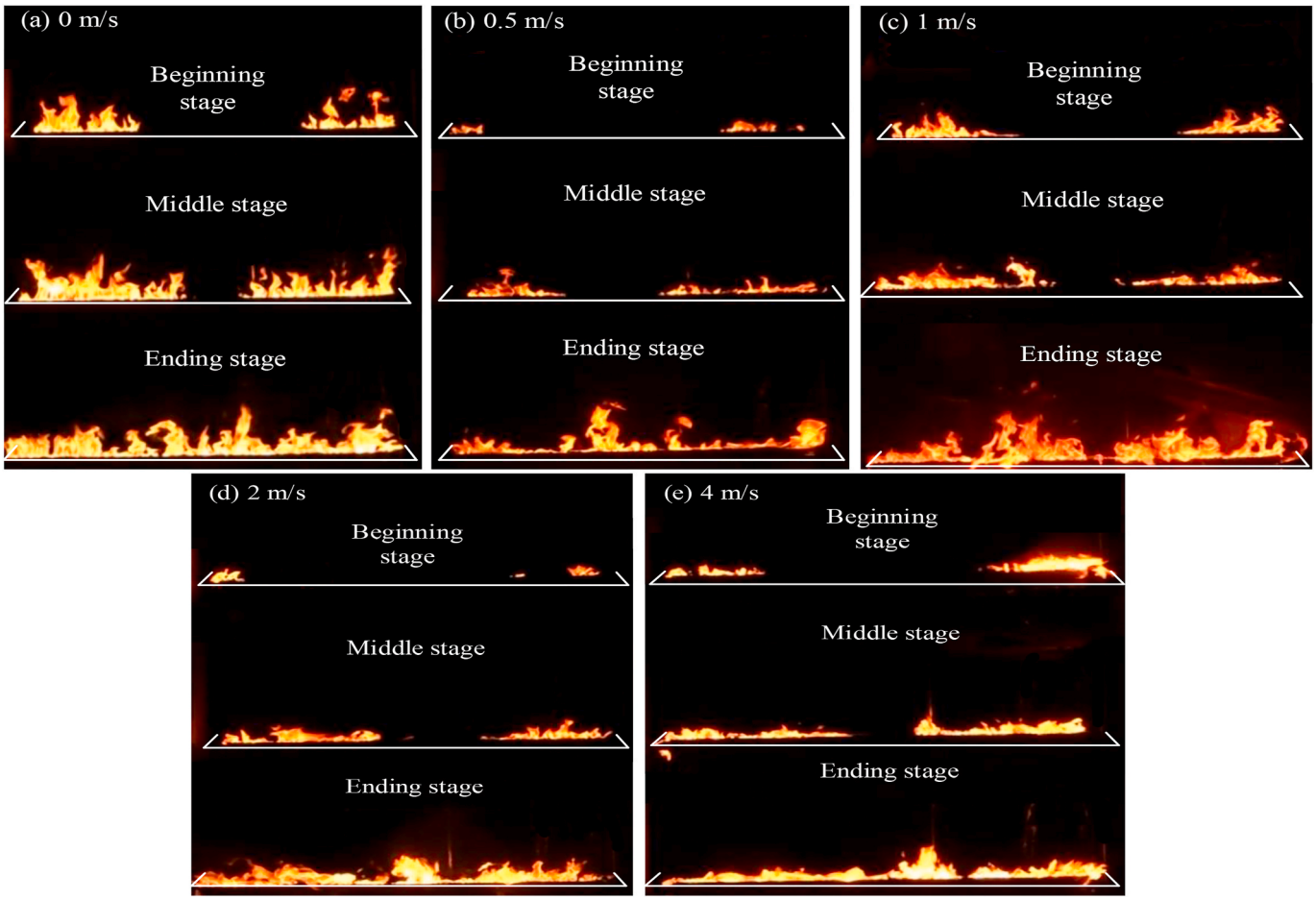

Fig. 3. The instantaneous flame spread images under perpendicular wind (front-view).

substrate will be further investigated in future studies. Furthermore, the pool sidewalls used in this study (height of 5 cm) are designed to minimize extraneous variables (e.g., fuel dispersion, unconfined flow). A sidewall-free setup introduces uncontrolled variations in fuel flow, precluding unambiguous attribution of observed flame behavior in wind. Given the high flashpoint of RP-5 (about 74 °C), 15 cm-long gasoline ignition zones were reserved at both pool ends (Fig. 1b). Gasoline was injected into these zones and torch-ignited at experiments commencement. The pool was centered within the test section of a combustion wind tunnel (1.8 m × 1.8 m × 6 m) that could provide 0–10 m/s uniform airflow with turbulence intensity controlled within ±4% [26,27]. Based on preliminary tests, three wind directions (concurrent, opposed, and perpendicular) and five constant airflow speeds (0, 0.5, 1, 2, and 4 m/s) were selected. Two CCD cameras (SONY FDR-AX45, 50 fps) were positioned perpendicularly along the pool's long and short axes to record real-time flame morphology evolution. A K-type armored thermocouple array (sheath diameter: 1 mm, range: 0–1050 °C) with 7.5 cm spacing was installed at the pool center. The array was divided into two groups: TC-1 to TC-5 measured gas-phase temperature 5 mm above the fuel surface, while TC-6 to TC-10 measured liquid-phase temperature at the fuel surface [28,29]. Thermocouples were inserted parallel to the fuel surface from the pool side to minimize flow disturbance [30]. Each case was repeated 3 times for data stability. After each case, contaminated water was replaced with fresh water to maintain consistent initial conditions. The ambient air temperature was maintained at 10 ± 2 °C with a relative humidity of 24 ± 4%.

3. Results and discussion

3.1. Flame spread behavior

3.1.1. Flame spread behavior in parallel wind ($u_{\parallel}$)

Fig. 2 presents the typical merging process of dual flames spreading toward each other under parallel wind ($u_{\parallel}$), where one flame is concurrent spread, and the other is opposed spread (see Videos S1 and S2). Three evolutionary stages—beginning stage, middle stage, and ending stage (flame merging)—are analyzed per experimental scenario. Beginning stage means the flames start to spread from the 15 cm ignition zones at both ends of the fuel pool; Middle stage means the flames spread to 1/2 of the length of fuel pool; and Ending stage means the flame merging occurs. Overall, as wind speed ($u_{\parallel}$) increases, flames on both sides progressively tilt along the airflow direction (blue arrows), with higher u values corresponding to an increased proportion of flame adhering to the fuel surface. At $u_{\parallel}$ = 4 m/s, flames spread quasi-horizontally along the liquid interface. Additionally, clustered vertical or inclined flamelets observed (e.g., Fig. 2b) during low airflow speed gradually diminish with increasing $u_{\parallel}$. Comparative analysis reveals symmetrical flame behaviors at u = 0, while directional divergence emerges when $u_{\parallel} > 0$: the right-side flame (concurrent wind) exhibits reduced height due to wind-induced horizontal inertia, with flame splitting at its leading edge when $u_{\parallel} > 1$ m/s (marked with red ovals in Fig. 2) [21]; the left-side flame (opposed wind) demonstrates fuel vapor accumulation toward the left boundary, enlarging flame volume near the pool edge while advancing uniformly with stable spread characteristics (as indicated by the red arrows).

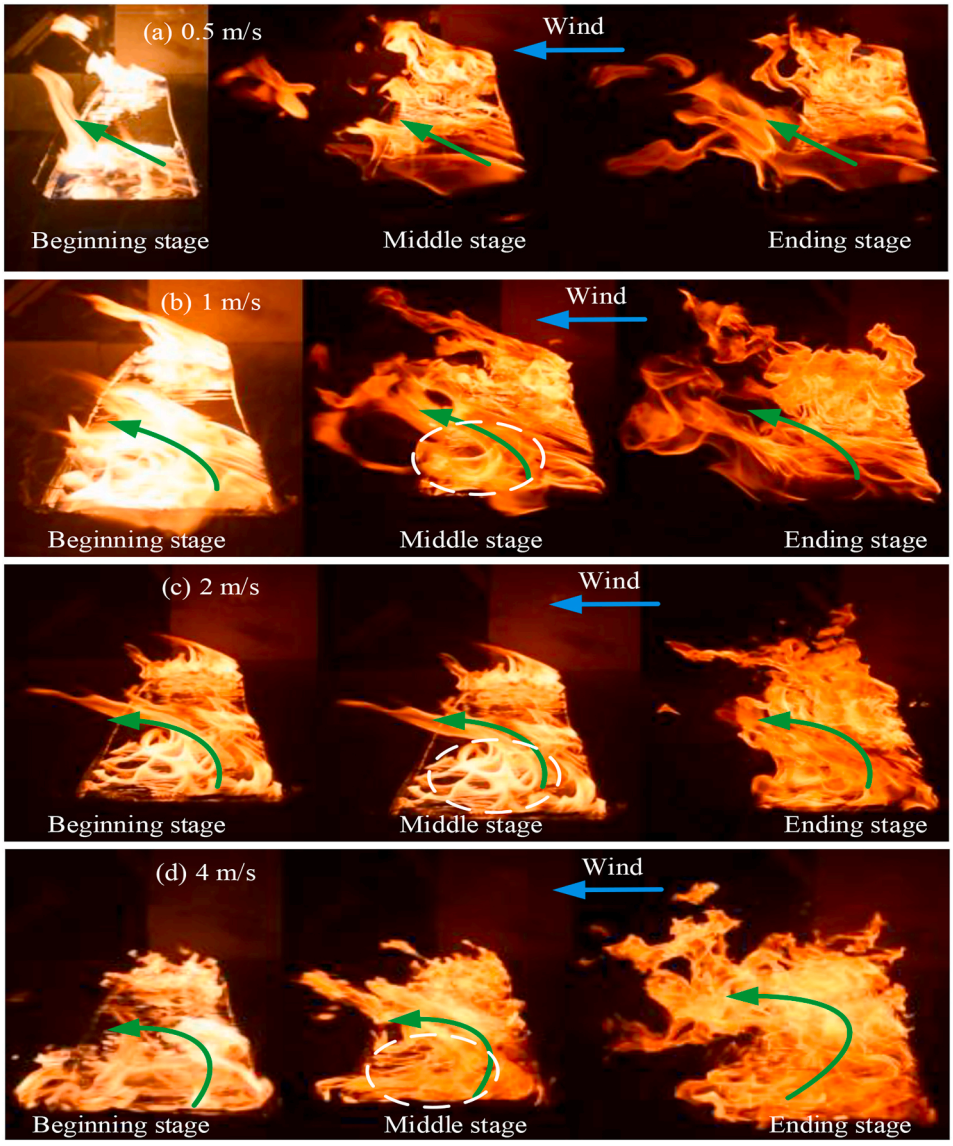

Fig. 4. The instantaneous flame spread images under perpendicular wind (side-view).

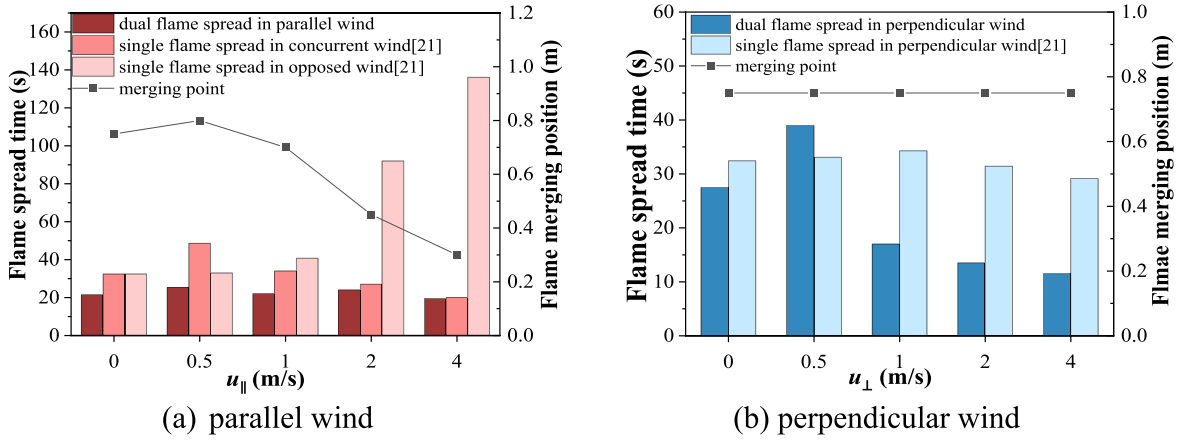

Fig. 5. Variation of flame spread time and merging point position with wind speed.

3.1.2. Flame spread behavior in perpendicular wind ($u_{\perp}$)

Figs. 3 and 4 display characteristic front-view and side-view images of two flames spreading towards merging under perpendicular wind ($u_{\perp}$). Fig. 3 reveals symmetrical flame spread behaviors on both sides of

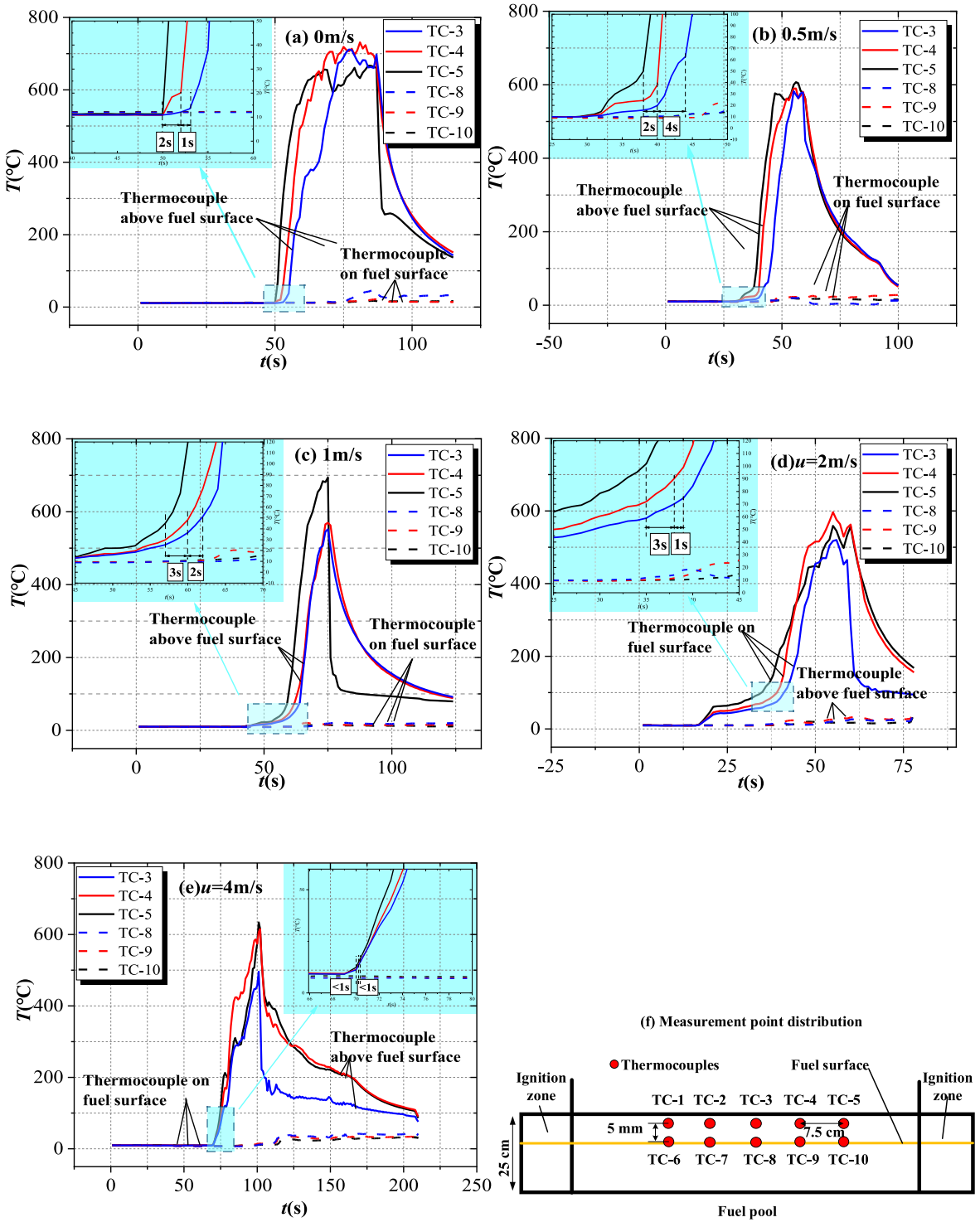

Fig. 6. T at different positions under parallel wind ($u_{\parallel}$).

the pool. To directly observe airflow effects, flame spread from the side perspective (Fig. 4) is analyzed, showing that increasing u significantly enhances local flame turbulence and transitions flame pulsation toward chaotic behavior (also see Video S3). Specifically, when $u_{\perp} \leq 0.5$ m/s, flames tilt downstream with the airflow while maintaining stable overall morphology. As $u_{\perp} > 0.5$ m/s, rotational tilting around the fuel surface occurs (green arrows), forming symmetric vortex structures (white dashed ellipses). These observations confirm a critical wind speed beyond which abrupt morphological transitions occur in dual-flame spread and merging, which is similar to single-flame spread phenomena reported by Mao et al. [21]. It can be concluded that reducing or eliminating the sidewall height will reduce—even eliminate—the formation of symmetric vortex structures and rotational flame tilting under high-velocity perpendicular wind conditions, as this modification disrupts the lateral confinement and flow symmetry essential for these phenomena.

3.2. Flame spread time

Fig. 5 characterizes the effects of wind speed (u) and wind direction

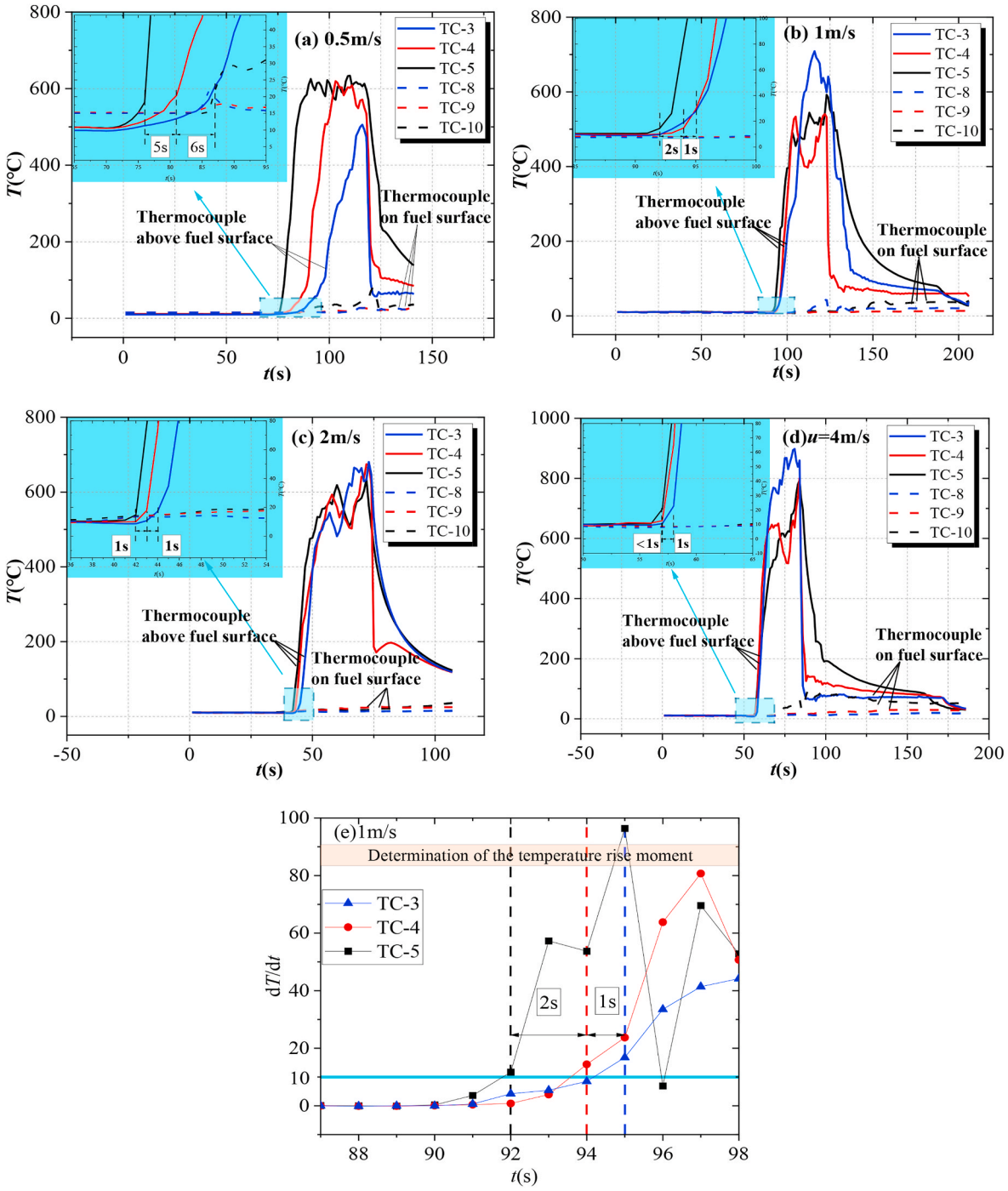

Fig. 7. T at different positions under perpendicular wind ($u_{\perp}$).

(θ) on dual flame spreading and merging by presenting flame spread times and corresponding merging point locations. Under the parallel wind ($u_{\parallel}$), dual flame spread times (the duration from ignition to merging, quantified over the 1.2 m central fuel length (excluding 15 cm ignition zones)) are consistently lower than cases of single-flame spread [21], exhibiting oscillatory variations within 21.22% as u increases. Notably, maximum spread time occurs at $u_{\parallel} = 0.5$ m/s, with the merging point positioned 0.8 m from the pool's left end (total length: 1.5 m, including 15 cm ignition zones at both left and right ends). This right-of-center merging indicates a higher spread rate on the left (opposed wind) side, attributable to momentum-driven fuel vapor migration from the combustion zone (right) to the unburned region (left) at $u_{\parallel} \leq 0.5$ m/s. This process depletes vapor in the right combustion zone, reducing local burning intensity, while vapor accumulation on the left fuel surface—resulting from right-flame shielding and vapor migration-mitigates the decline in left-side flame spread rate. When $u_{\parallel} > 0.5$ m/s, airflow-induced kinetic energy dominates over thermal buoyancy in governing fire spread behavior. The left-side flame front exhibits low temperature, thereby reducing convective heat transfer efficiency and leading to a decrease in the flame spread rate. Simultaneously, the right-side flame undergoes stretch-induced augmentation of the burning region, leading to a marked increase in flame spread rate. At $u_{\parallel} = 4$ m/s, this causes a 62.5% leftward displacement of the merging point compared with the scenario at 0.5 m/s, positioning it merely 0.3 m from the left edge of the fuel pool,

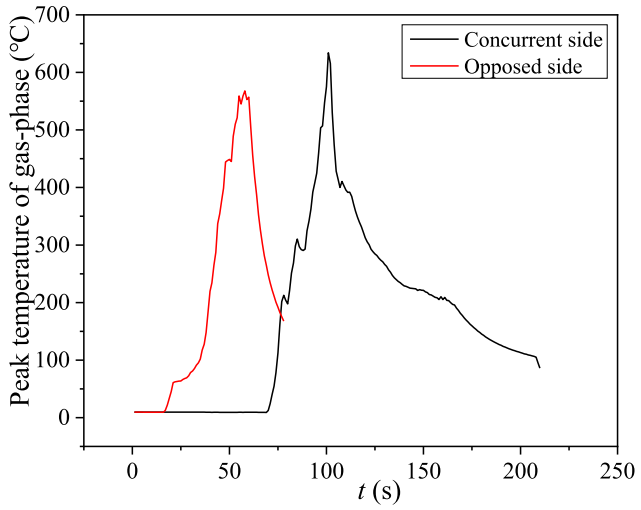

Fig. 8. Peak temperatures of gas-phase under parallel wind ($(u_{\parallel} = 4$ m/s).

which corresponds to 0.15 m from the boundary between the left ignition zone and the non-ignition central region. This phenomenon reveals the dynamic competition mechanism between two flames in parallel wind as wind speed varies.

For the perpendicular wind ($u_{\perp}$) shown in Fig. 5b, the flame merging point remains consistently centered at 0.75 m from the pool's left edge, indicating symmetrical propagation maintained by perpendicular wind. Dual flame spread time follows a non-monotonic trend with wind speed: peaking at 39 s when $u_{\perp} = 0.5$ m/s, then plummeting 70.5% as u reaches to 4 m/s. In contrast, single-source flame spread time in perpendicular wind varies within 16%, demonstrating stable characteristics. This divergence stems from fundamental mechanistic differences. Single source flame spread maintains stable oxygen entrainment and heat feedback along a single thermal plume path, avoiding significant fuel vapor accumulation. For dual flame spread at low speeds ($u_{\perp} \leq 0.5$ m/s), the collision of opposing thermal plumes weakens the transfer of radiative heat flux through multiple interrelated mechanisms, ultimately leading to prolonged flame spread time. The specific action paths are as follows: Firstly, the collision directly disrupts the concentrated state and directional propagation law of high-temperature radiative components — the high-temperature radiative components that should have been concentrated toward the unburned fuel surface between the two flames undergo multidirectional scattering and diffusion due to the collision. This results in a significant reduction in the local concentration of radiative components above the unburned fuel, directly weakening the intensity of radiative heat flux reaching the fuel surface. Secondly, the mutual interaction forces generated by the plume collision force the thermal plumes to deflect laterally, pushing the high-temperature radiative sources away from the unburned fuel surface. This not only increases the effective distance of radiation propagation but also requires the radiation path to pass through a thicker layer of ambient cold air. Finally, the absorption and scattering effects of cold air on thermal radiation (especially the medium and long-wave radiation emitted by high-temperature combustion products) are significantly enhanced, further exacerbating the attenuation of radiative heat flux. These aforementioned effects also explain the prolonged flame spread time observed in experiments under low perpendicular wind speeds. When $u_{\perp} > 0.5$ m/s, enhanced turbulence intensity accelerates fuel-oxygen mixing, increasing reaction rates. Simultaneously, vortex structures formed by dual flame fronts direct high-temperature products toward unburned regions efficiently, elevating preheating efficiency and accelerating

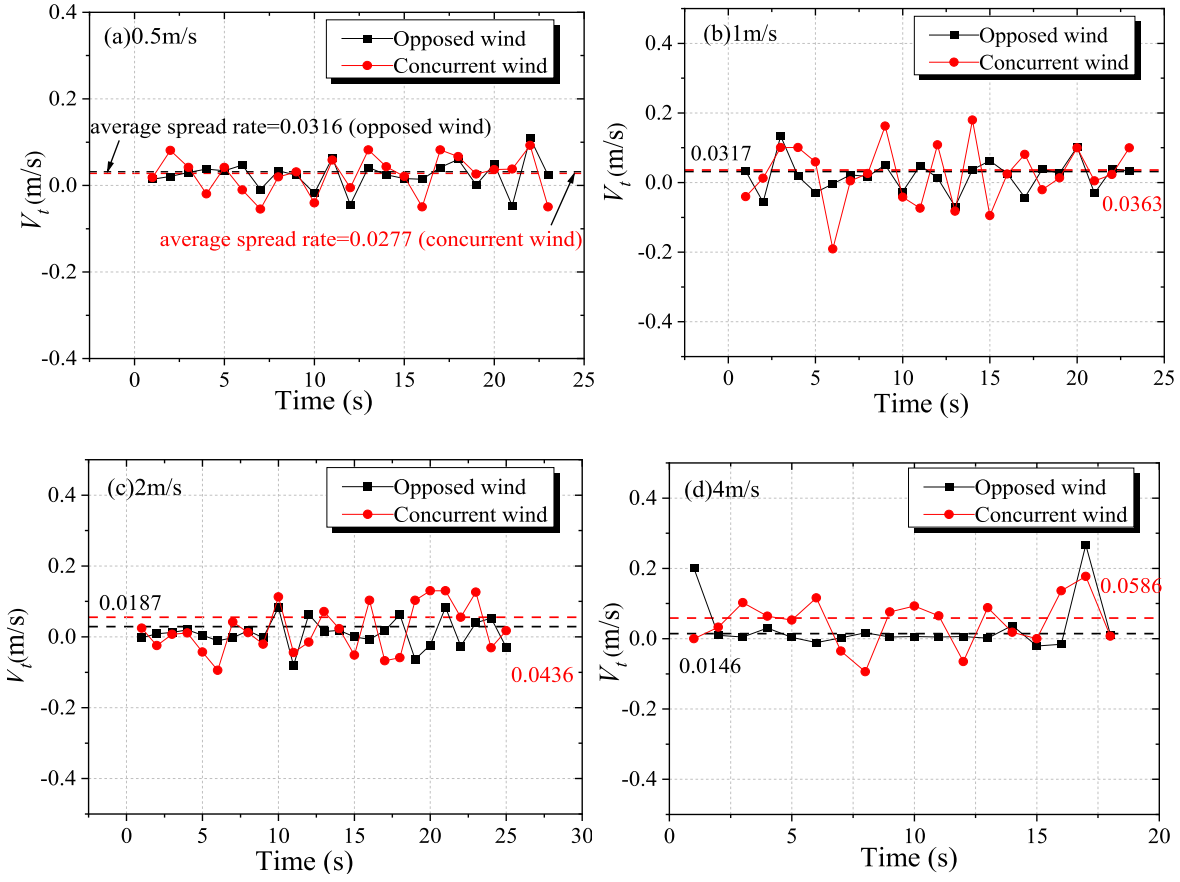

Fig. 9. Transient flame spread rate V_t of two opposite-spreading flames under parallel wind.

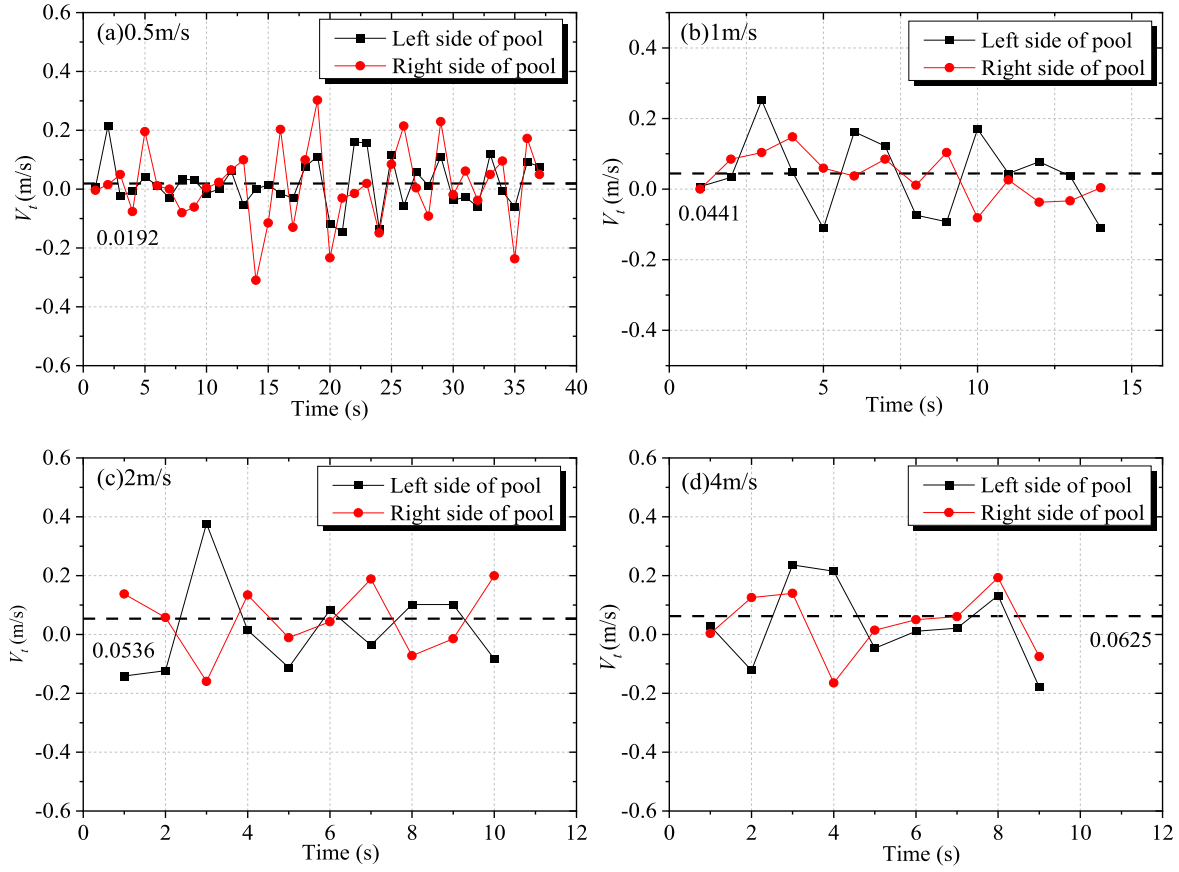

Fig. 10. Transient flame spread rate V_t of two opposite-spreading flames under perpendicular wind.

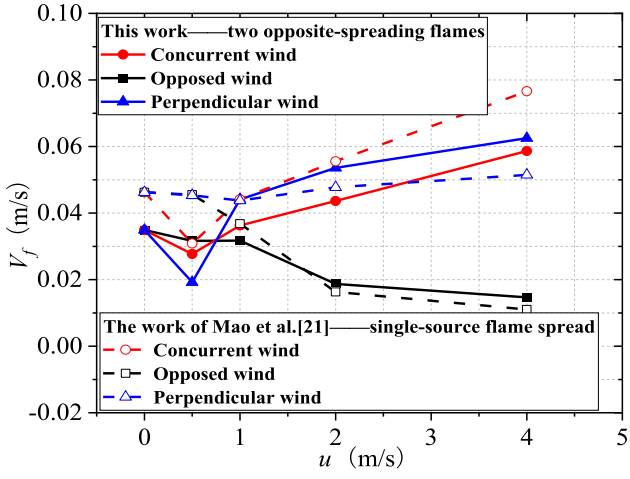

Fig. 11. Correlation between average flame spread rate V_f and wind speed u.

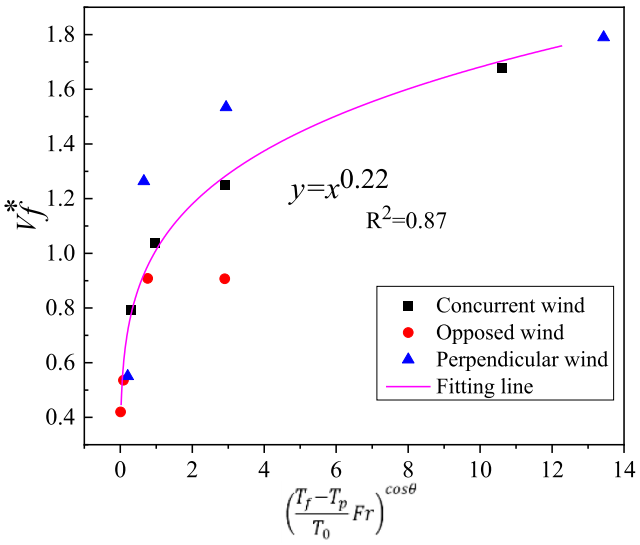

Fig. 12. V_f^* under various wind conditions.

spread. This wind-speed threshold effect reveals the unique "inhibition-promotion transition mechanism" characteristic of dual flame spread in $u_\perp$.

3.3. Gas-liquid temperature distribution

Figs. 6 and 7 present time-dependent temperature profiles (T) of thermocouples at gas-liquid interface positions under parallel and perpendicular winds. Considering the symmetry of the fuel pool and to minimize boundary effects, near-center thermocouples are selected for analysis: TC-3, TC-4, TC-5 (gas-phase, 5 mm above the fuel surface) and TC-8, TC-9, TC-10 (liquid-phase, at the fuel surface). The determination of the temperature rise moment is based on the characteristic of the instantaneous rate of increase (dT/dt) in the temperature-time curve. The specific criterion is as follows: when the instantaneous rate of increase exceeds 10 °C/s, the corresponding moment is regarded as the starting point of temperature rise. As shown in Fig. 7 (e), the temperature increase rates of TC-3, TC-4, and TC-5 exceed 10 °C/s threshold at t = 92s, t = 94s, and t = 95s, respectively. Therefore, t = 92s, t = 94s, and

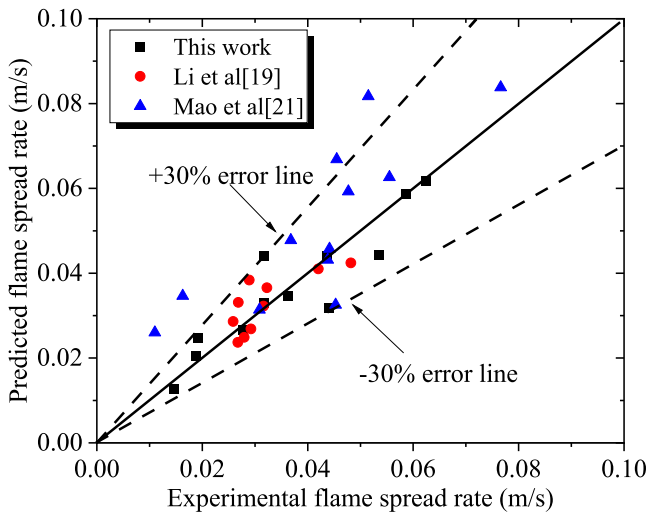

Fig. 13. Comparison of experimental value and predicted value.

Table 1
Uncertainty of temperature and flame spread rate.

Parameters	Uncertainty source	Uncertainty value	Final uncertainty
Temperature	radiation error	±4.0%	±9.03%
	repeatability error	±8.1%	
Flame spread rate	repeatability error	±6.9%	±8.03%
	measurement error	±4.1%	

$t = 95$s are regarded as the starting points of temperature rise, resulting in temperature rise intervals of 2s (between TC-3 and TC-4) and 1s (between TC-4 and TC-5).

Results demonstrate significantly earlier temperature rise in the gas-phase than liquid-phase: gas-phase thermocouples exhibit rapid transient responses (600–800 °C peak within seconds) due to direct flame heating, while liquid-phase temperatures rise gradually, generally not exceeding 100 °C. Compared to no-wind conditions, temperature rise intervals extend universally at $u = 0.5$ m/s, confirming low-speed airflow suppression of flame spread. With increasing wind speed, the temperature rise intervals between adjacent thermocouples are further shortened, indicating an accelerated flame spread rate. This acceleration is mainly attributed to the forced airflow tilting the flame towards the unburned fuel surface, enhancing radiative heat transfer to the leading edge region. As a result, fuel is preheated and vaporized earlier than under low-speed conditions, rapidly forming flammable vapor concentrations near the fuel surface to sustain spread. Consequently, convective heat transfer dependence weakens, with propagation increasingly governed by radiation and airflow-transported fuel vapors. Moreover, the evolution of thermocouple temperature rise intervals under different wind directions directly reflect dynamic responses in flame spread rate. At $u_\perp \leq 0.5$ m/s, the temperature rise intervals under perpendicular wind conditions are prolonged due to the collision of thermal plumes, indicating a reduced flame spread rate. Conversely, when $u_\perp > 0.5$ m/s, the temperature rise intervals under perpendicular wind shorten dramatically, with reduction amplitudes exceeding those in concurrent wind scenarios. This demonstrates the superior acceleration effect of high-speed perpendicular wind on flame spread, while the growth of fire spread under concurrent wind remains constrained.

Furthermore, under parallel wind ($u_\parallel = 4$ m/s), as shown in Fig. 8, the peak temperature of gas-phase thermocouples on the concurrent side is about 70 °C higher than that on the opposed side. The difference in temperature gradients directly reflects variations in combustion intensity and oxygen consumption, providing quantitative support for the influence of airflow consumption on flame dynamics.

Combining the data of the gas-phase temperatures and flame spread times, under perpendicular wind ($u_\perp = 4$ m/s), the peak gas-phase temperatures are higher than those under parallel wind at the same speed (Figs. 6e and 7d), and the flame spread time is shortened by nearly 41% (Fig. 5). These two sets of data collectively confirm more intense combustion under perpendicular wind.

3.4. Flame spread rate

Figs. 9 and 10 present transient flame spread rates V_t under various wind directions and speeds, defined as the propagation distance of the flame tip per unit time. For clarity, dashed lines of average spread rates are included. V_t oscillates around these dashed lines, indicating pulsating propagation along the fuel surface – a phenomenon primarily linked to fluctuations in fuel vapor concentration. Owing to the forward and reverse pulsations of the flames, the transient spread rates exhibit both positive and negative values. During initial combustion, vapor concentration near the lower flammability limit fluctuates due to low initial fuel temperature; when the concentration exceeds this limit, flames surge forward, forming pulsating propagation. Wind direction significantly modulates transient spread characteristics: under perpendicular wind, V_t exhibits the largest fluctuation amplitude (instantaneous peaks exceeding 0.2 m/s), reflecting strong perturbation by wind disturbances. Conversely, opposed wind conditions markedly reduce V_t and fluctuation intensity, as wind blows fuel vapor toward the upstream direction of fire source, depleting vapor concentration at the flame front and inhibiting forward propagation.

Fig. 11 illustrates trends in average flame spread rate V_f of two opposite fires under different wind directions and speeds. The data of V_f are expressed as absolute values, which is primarily intended to facilitate comparisons of spread rate magnitudes; no directional information is specified in this representation. At low wind speeds ($u \leq 0.5$ m/s), V_f universally decreases due to airflow removing fuel vapor and cooling the flame front's high-temperature liquid layer, suppressing sustained propagation. For $u > 0.5$ m/s, a direction-dependent divergence in V_f emerges: Concurrent wind conditions accelerate V_f through flame stretching that expands combustion area and intensifies radiative heat transfer, enhancing fuel preheating and vaporization. Perpendicular wind, despite directional misalignment, enhances flame-surface heat exchange and vapor transport ahead of flames, increasing spread rate. Opposed wind constrains flame expansion and reduces spread. These trends align with observations by Mao et al. [21] under single-source ignition conditions, though their study reported limited sensitivity of flame propagation to perpendicular wind. In contrast, the present work demonstrates that two oppositely spreading flames exhibit superior sensitivity to perpendicular wind, with V_f increases surpassing those under concurrent wind conditions. This enhanced responsiveness arises from the orthogonal wind's induction of symmetric flame dynamics: high-speed symmetric shear layers develop orthogonal to the spread direction, intensifying turbulent mixing while uniformly distributing fuel vapor-oxygen mixtures. This creates a stable, fuel-rich combustion environment that amplifies heat feedback to the fuel surface. Concurrently, flame radiation from two opposite fires superimposes in the central region, boosting liquid surface preheating. This dual turbulence-thermal coupling makes flame spread rate highly sensitive to perpendicular wind speed, particularly accelerating at high speeds.

Conversely, asymmetric concurrent wind and opposed wind interaction in parallel fields trigger bidirectional competition. Concurrent wind transports fuel vapor downstream while the opposed wind flame simultaneously attempts to spread oppositely, causing oxygen competition between the two flame fronts. Moreover, heat and fuel vapor are dynamically allocated between two opposite flames. Consequently, the concurrent wind flame cannot fully exploit the wind's advantage as in single-source flame spread, thereby limiting its spread rate. In single-source flame spread, the absence of an opposing flame allows airflow to act solely on a single flame front. This not only enhances directional

mixing of fuel vapor and oxygen but also expands the combustion surface area via flame stretching, leading to sustained acceleration of the flame spread rate.

Under windy conditions, flame spread is governed by the combined effects of ambient wind inertia and fire-induced thermal buoyancy, exhibiting airflow-dominated propagation behavior. To quantitatively characterize wind's role, the dimensionless Froude number (Fr) is introduced to represent the ratio of wind inertial force to thermal buoyancy [31]: $Fr = \frac{u^2}{gL}$, where g denotes gravitational acceleration (9.8 m/s^2). L refers to the horizontal distance of one side flame from its ignition zone to the flame merging point. Wind affects spread rate (distribution of L on each side) but not total spread length. By adjusting the magnitude of Fr, L determines whether the flame morphology is buoyancy-dominated (upright) or wind-dominated (tilted, split, or vortex-structured). Beyond wind parameters, initial fuel temperature T_0 significantly affects average flame spread rate V_f [32]: high T_0 increases initial vapor concentration above the fuel surface and reduces heat required to reach the flash point, thereby accelerating flame propagation [29]. The flame temperature T_f impacts V_f as established in prior studies [33,34]. T_f is measured using K-type thermocouples placed 5 mm above the fuel surface. It represents the spatial average of temperatures from measurement points within the flame spread region, aimed at mitigating short-term fluctuations and wind-induced horizontal temperature inhomogeneities. Additionally, the flash point (T_p) as an important fuel property is also considered as one of the parameters in the correlation. To facilitate analysis of wind speed effects, the average flame spread rate in windless conditions $V_{f,u=0}$ is referenced to define the dimensionless average flame spread rate V_f^* as:

$$V_f^* = V_f \Big/ V_{f,u=0} \tag{1}$$

For various wind conditions, V_f depends not only on wind speed u but also on wind direction θ (relative to the spread direction). A directional factor $\cos\theta$ (where $\cos\theta = 1$ for concurrent and perpendicular wind, $\cos\theta = -1$ for opposed wind) is introduced to quantify directional effects. Integrating key parameters, V_f^* under parallel wind is expressed as:

$$V_f^* = fcn\left(Fr, T_0, T_f, T_p, \theta\right) \tag{2}$$

From physical mechanisms, the thermal driving force for flame spread depends on two key temperature differences: (T_f -T_p) represents the "excess thermal energy" of the flame relative to the fuel's flash point. (T_p -T_0) represents the "thermal barrier" that the fuel must overcome to reach the flash point from its initial state. The ratio (T_f -T_p)/(T_p -T_0) encapsulates the net thermal driving potential for flame spread—integrating both the available thermal energy from the flame and the thermal resistance of the fuel itself. By combining the above components (Fig. 12), the dimensionless average flame spread rate V^*_f is derived via experimental fitting:

$$V_f^* = \left(\frac{T_f - T_p}{T_p - T_0} Fr\right)^{0.22\cos\theta} \quad 2.72 > Fr > 0.019 \tag{3}$$

To assess the validity of Eq. (3), the predicted single-source flame spread rates have been juxtaposed with experimental data obtained from literature [19,21], as depicted in Fig. 13. Specifically, Li et al. [19] experimentally studied diesel flame spread under concurrent wind and opposed wind conditions (0–2.065 m/s). The diesel flame temperatures in Li et al. [19] are estimated using those from this work under similar wind speeds. Mao et al. [21] investigated RP-5 aviation kerosene flame spread under varied forced airflow speeds (0–6 m/s) and directions (concurrent wind, opposed wind, perpendicular wind). Results demonstrate that, for the forced airflow range ($2.72 > Fr > 0.019$) and fuels with similar combustion characteristics, errors between the predicted and experimental values of V_f within 30%. The 30% verification error arises from the cumulative effects of experimental measurement limitations, model simplifications to complex physics, and inherent variability in dual-flame spread dynamics. These findings confirm the reliability of the proposed prediction model, particularly for parallel and perpendicular wind scenarios under forced ventilation.

4. Conclusions

Aviation kerosene is widely used in aerospace and other critical sectors. When accidental fuel leakage and combustion occur, the flame spread process is significantly affected by ambient wind, and intense radiation frequently causes multiple ignition sources to spread simultaneously, leading to severe thermal hazards. To address these risks and enhance scientific fuel safety management, this study experimentally examined the effects of wind speed u (0–4 m/s) and wind direction θ (concurrent, opposed and perpendicular winds) on spread and merging behaviors of two opposite flames over RP-5 aviation kerosene. The main conclusions include:

(1) Flame spread behavior exhibits significant variations with wind speed and direction. Flame tilting consistently aligns with airflow direction. At $u \leq 0.5$ m/s, flame spread remains stable. When $u >$ 0.5 m/s, direction-dependent morphological transitions emerge: Concurrent wind induces flame splitting at the leading edge, driven by shear-induced stretching of the flame front. Perpendicular wind triggers rotational deflection of the flame around the fuel surface, accompanied by the formation of symmetric vortex structures in the flow field. Opposed wind results in steady uniform propagation, with minimal morphological distortion.

(2) Under parallel wind, flame spread time shows oscillatory variations with u, with the merging point progressively shifting toward the opposed wind side. For perpendicular wind, the merging point remains centered, while spread time first increases then decreases with wind speed, peaking at $u = 0.5$ m/s. Gas-liquid temperature distributions reveal heat transfer dynamics: gas-phase temperatures surge rapidly, liquid-phase responses lag. Both spread time and temperature rise intervals extend at $u \leq 0.5$ m/s versus no-wind conditions, confirming the inhibitory effect of low wind speed on flame spread.

(3) Transient flame spread rates V_t exhibit pulsating fluctuations around mean values, indicating unsteady propagation. Among all wind directions, the "turbulence-thermal" dual coupling effect induced by perpendicular wind makes the V_t highly sensitive to perpendicular wind speed (instantaneous peaks exceeding 0.2 m/s), while opposed wind substantially reduces instantaneous rates and fluctuations. For average flame spread rates V_f, directional differences are minimal at $u \leq 0.5$ m/s, with all configurations exhibiting comparable V_f; at $u > 0.5$ m/s, concurrent and perpendicular wind significantly accelerate spread, whereas opposed wind suppresses it. Integrating key parameters (wind speed, wind direction, initial fuel temperature, flame temperature), a prediction model for V_f under parallel and perpendicular wind conditions is developed, with particular suitability for bidirectional flame spread of RP-5 aviation kerosene.

CRediT authorship contribution statement

Bo Li: Writing – review & editing, Funding acquisition, Conceptualization. **Yangjin Shi:** Writing – original draft, Data curation. **Xinyan Huang:** Writing – review & editing, Supervision. **Asif Sohail Usmani:** Supervision, Project administration, Funding acquisition.

Declaration of competing interest

The authors declare that they have no known competing financial interests or personal relationships that could have appeared to influence the work reported in this paper.

Acknowledgment

This work was supported by the National Natural Science Foundation of China (NSFC, Grant Nos. 52036009 and 52206179), Opening Fund of National & Local Joint Engineering Research Center of Thermal Safety Technology (erctst2023-KF01), and Hong Kong Scholars Program under Grant No. XJ2024027. XH thanks the support from State Key Laboratory Of Climate Resilience For Coastal Cities (SKL-CRFCC).

Appendix

The uncertainty analysis follows the methodology proposed by Moffat [35], where the total uncertainty is estimated as the root sum of squares (RSS) of all error sources. As documented in Table 1, the final uncertainties for temperature and flame spread rate are calculated to be ±9.03% and ±8.03%, respectively.

Appendix A. Supplementary data

Supplementary data to this article can be found online at https://doi.org/10.1016/j.firesaf.2026.104843.

References

[1] J. Zhao, S. Lu, Y. Fu, M.U. Shahid, H. Zhang, Application of ultra-fine dry chemicals modified by POTS/OBS for suppressing aviation kerosene pool fire, Fire Saf. J. 118 (2020) 103148, https://doi.org/10.1016/j.firesaf.2020.103148.
[2] J.T. Leonard, C.R. Fulper, R. Darwin, G.G. Back, R.E. Burns, Fire Hazards of Mixed Fuels on the Flight Deck, Naval Research Lab., Washington, DC (United States, 1992.
[3] M. Li, S. Lu, J. Guo, K.L. Tsui, Study on flame spread over aviation kerosene and diesel, Adv. Mater. Res. 1016 (2014) 587–591. https://doi.org/10.4028/www.scientific.net/AMR.1016.587.
[4] F. Tang, L. Li, Q. Wang, Q. Shi, Effect of cross-wind on near-wall buoyant turbulent diffusion flame length and tilt, Fuel 186 (2016) 350–357, https://doi.org/10.1016/j.fuel.2016.08.095.
[5] H. Li, J. Liu, J. Ge, Phenomenological characteristics of continuous spill fires in a tunnel with longitudinal ventilation, Process Saf. Environ. Prot. 138 (2020) 108–116, https://doi.org/10.1016/j.psep.2020.03.010.
[6] K. Åtland, T. Nilsen, T. Pedersen, Military muscle-flexing as interstate communication: russian NOTAM warnings off the Coast of Norway, 2015–2021, Scandinavian Journal of Military Studies 5 (2022) 63–78, https://doi.org/10.31374/sjms.133.
[7] H.E. Anderson, R.C. Rothermel, Influence of moisture and wind upon the characteristics of free-burning fires, Symposium (International) on Combustion 10 (1965) 1009–1019, https://doi.org/10.1016/s0082-0784(65)80243-0.
[8] M. Li, Z. Shu, S. Geng, G. Han, Experimental and modelling study on flame tilt angle of flame spread over jet fuel under longitudinally forced air flows, Fuel 270 (2020) 117516, https://doi.org/10.1016/j.fuel.2020.117516.
[9] M. Li, Z. Shu, B. Chen, C. Wang, S. Geng, G. Han, Influence of pool width on pioneering flame height of flame spread over jet fuel inside a bench-scale air flow tunnel, Tunn. Undergr. Space Technol. 108 (2021) 103763, https://doi.org/10.1016/j.tust.2020.103763.
[10] J.H. Burgoyne, A.F. Roberts, The spread of flame across a liquid surface II. Steady-state conditions, Proceedings of the Royal Society of London. Series A. Mathematical and Physical Sciences 308 (1968) 55–68, https://doi.org/10.1098/rspa.1968.0207.
[11] T. Suzuki, T. Hirano, Flame propagation across a liquid fuel in an air stream, Symposium (International) on Combustion 19 (1982) 877–884, https://doi.org/10.1016/S0082-0784(82)80263-4.
[12] V.V. Zamashchikov, Flame spread across shallow pools in modulated opposed air flow in narrow tube, Combust. Sci. Technol. 181 (2008) 176–189, https://doi.org/10.1080/00102200802424484.
[13] S. Mansoor Ali, V. Raghavan, K. Velusamy, S. Tiwari, A numerical study of concurrent flame propagation over methanol pool surface, J. Heat Tran. 134 (2012) 041202, https://doi.org/10.1115/1.4005111.
[14] N. Zhu, X. Huang, J. Fang, L. Yang, L. Hu, Transitional flame-spread and fuel-regression behaviors under the change of concurrent wind, Fire Saf. J. 120 (2021) 103015, https://doi.org/10.1016/j.firesaf.2020.103015.
[15] M.J. Gollner, C.H. Miller, W. Tang, A.V. Singh, The effect of flow and geometry on concurrent flame spread, Fire Saf. J. 91 (2017) 68–78, https://doi.org/10.1016/j.firesaf.2017.05.007.
[16] Z. Mao, Z. Xia, B. Li, S. Mao, C. Zhou, D. Zhang, Y. Zhou, Experimental study of gas-liquid phase temperature distribution and heat transfer behavior in flame spread over jet fuel with forced airflow, Int. J. Therm. Sci. 210 (2025) 109640, https://doi.org/10.1016/j.ijthermalsci.2024.109640.
[17] H.D. Ross, F.J. Miller, Flame spread across liquid pools with very low-speed opposed or concurrent airflow, Symposium (International) on Combustion 27 (1998) 2723–2729, https://doi.org/10.1016/S0082-0784(98)80128-8.
[18] J. Zanganeh, B. Moghtaderi, Flame spread over porous sand beds wetted with propenol, Fire and materials 35 (2011) 61–70, https://doi.org/10.1002/fam.1035.
[19] M. Li, C. Wang, Z. Li, S. Yang, K. Fukumoto, C. Fan, Combustion and flame spreading characteristics of diesel fuel with forced air flows, Fuel 216 (2018) 390–397, https://doi.org/10.1016/j.fuel.2017.11.100.
[20] X. Huang, J. Gao, A review of near-limit opposed fire spread, Fire Saf. J. 120 (2021) 103141, https://doi.org/10.1016/j.firesaf.2020.103141.
[21] S. Mao, Z. Mao, B. Li, W. Hao, S. Liu, Y. Hu, Experimental study on behaviors of flame spread over aviation kerosene under forced airflow, Process Saf. Environ. Prot. 168 (2022) 768–777, https://doi.org/10.1016/j.psep.2022.10.041.
[22] N. Liu, J. Lei, W. Gao, H. Chen, X. Xie, Combustion dynamics of large-scale wildfires, Proc. Combust. Inst. 38 (2021) 157–198, https://doi.org/10.1016/j.proci.2020.11.006.
[23] R. Wadhwani, D. Sutherland, K. Moinuddin, X. Huang, Numerical simulation of two parallel merging wildfires, Int. J. Wildland Fire 32 (2023) 1726–1740, https://doi.org/10.1071/WF23071.
[24] C.M. Thomas, J.J. Sharples, J.P. Evans, Modelling the dynamic behaviour of junction fires with a coupled atmosphere–fire model, Int. J. Wildland Fire 26 (2017) 331–344, https://doi.org/10.1071/WF16079.
[25] N. Liu, Wildland surface fire spread: mechanism transformation and behavior transition, Fire Saf. J. 141 (2023) 103974, https://doi.org/10.1016/j.firesaf.2023.103974.
[26] B. Li, F. Ge, J. Ji, Experimental study on interaction mechanism on the mass burning rate in two n-heptane fires with cross airflows, Fire Safe J 134 (2022) 103676, https://doi.org/10.1016/j.firesaf.2022.103676.
[27] B. Li, H. Wan, Z. Gao, J. Ji, Experimental study on the characteristics of flame merging and tilt angle from twin propane burners under cross wind, Energy 174 (2019) 1200–1209, https://doi.org/10.1016/j.energy.2019.03.061.
[28] D. Schiller, H. Ross, W. Sirignano, Computational predictions of flame spread over alcohol pools, in: 31st Aerospace Sciences Meeting, 1993, https://doi.org/10.2514/6.1993-825.
[29] M. Li, S. Lu, R. Chen, J. Guo, C. Wang, Experimental investigation on flame spread over diesel fuel near sea level and at high altitude, Fuel 184 (2016) 665–671, https://doi.org/10.1016/j.fuel.2016.07.060.
[30] P. Vacca, E. Planas, C. Mata, J.A. Muñoz, F. Heymes, E. Pastor, Experimental analysis of real-scale burning tests of artificial fuel packs at the Wildland-urban interface, Saf. Sci. 146 (2022) 105568, https://doi.org/10.1016/j.ssci.2021.105568.
[31] L. Hu, A review of physics and correlations of pool fire behaviour in wind and future challenges, Fire Saf. J. 91 (2017) 41–55, https://doi.org/10.1016/j.firesaf.2017.05.008.
[32] W. Xie, Y. Zhang, J. Li, P. Mao, L. Chen, Experimental study on characteristics of flame spread over diesel and n-butanol pool fires in tunnel, Tunn. Undergr. Space Technol. 79 (2018) 286–292, https://doi.org/10.1016/j.tust.2018.05.017.
[33] D.N. Schiller, H.D. Ross, W.A. Sirignano, Computational analysis of flame spread across alcohol pools, Combust. Sci. Technol. 118 (1996) 203–255, https://doi.org/10.1080/00102209608951980.
[34] J.N. De Ris, Spread of a laminar diffusion flame, Symposium (International) on Combustion 12 (1969) 241–252, https://doi.org/10.1016/S0082-0784(69)80407-8.
[35] R.J. Moffat, Describing the uncertainties in experimental results, Exp. Therm. Fluid Sci. 1 (1988) 3–17, https://doi.org/10.1016/0894-1777(88)90043-X.